JACS
JOURNAL OF THE AMERICAN CHEMICAL SOCIETY
pubs.acs.org/JACS
Article

Ultraslow Relaxation of Toroidal State in Ferrotoroidal Dysprosium Complex

Deepanshu Chauhan, Sagar Paul,* Dipanti Borah, Appu Sunil, Wolfgang Wernsdorfer,* Maheswaran Shanmugam,* and Gopalan Rajaraman*

Cite This: J. Am. Chem. Soc. 2025, 147, 39572−39581
Read Online

ABSTRACT: Molecular systems are emerging candidates for quantum information science (QIS) due to their unique quantum behaviors and structural tunability, opening avenues for next-generation quantum technologies. While molecular nanomagnets (MNMs) have emerged as promising spin-based qubit candidates, achieving long coherence times and feasible readouts remains challenging. Among molecular nanomagnets, single-molecule toroics (SMTs) stand out as a particularly promising class, offering magnetically silent ground states, along with the unique ability to modulate their intrinsic chirality. Realizing toroidal states in molecular systems remains a significant hurdle, with the design and stabilization of ferrotoroidal (FT) moments posing an even greater level of complexity. Moreover, the anticipated slow relaxation of toroidal states has not been explicitly demonstrated, limiting their viability in molecular quantum devices. In this work, we report a tridecanuclear $[Ga_7Dy_6(N\text{-mdea})_6(ClCH_2COO)_6(NO_3)_6(OH)_{12}(H_2O)_6]\cdot 3Cl$ (**1**) complex, which exhibits an FT ground state. Remarkably, this complex shows slow relaxation of the toroidal states, experimentally observed for the first time, with a quantum tunneling of magnetization (QTM) relaxation time of $\sim 3.5 \times 10^8$ s (~11 years), far surpassing the relaxation times reported for state-of-the-art Dy(III) based single-molecule magnets. The robust FT ground state in complex **1** is unequivocally established by μSQUID and corroborated by *ab initio* calculations, marking a major advance in the field of SMTs. This ultraslow relaxation, arising from quenched many-body tunneling processes, lays the foundation for integrating toroidal states into quantum technologies and offers a new design paradigm for molecular complexes in QIS.

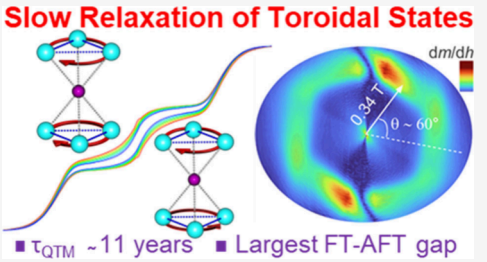

INTRODUCTION

Molecular magnets have emerged as promising platforms for quantum information science (QIS), owing to their well-defined spin states, long coherence times, and inherent structural tunability.[1] Among them, lanthanide-based complexes, particularly those featuring Dy(III), have attracted significant attention due to their strong magnetic anisotropy and large orbital angular momentum.[2,3] These properties underpin the phenomenon of single-molecule magnetism (SMM), where bistable magnetic states are separated by an energy barrier to spin reversal.[3] Landmark achievements, such as magnetic hysteresis in Dy(III) complexes above liquid nitrogen temperatures, underscore their technological potential.[4] Yet, the practical implementation of SMMs remains hindered by rapid quantum tunnelling of magnetization (QTM) and inefficient magnetic relaxation suppression mechanisms, factors that limit thermal stability and hinder reliable initialization and readout in quantum devices.[5] A transformative approach to overcoming these limitations is offered by single-molecule toroics (SMTs), a topological evolution of SMMs.[6,7] SMTs are characterized by vortex-like arrangements of local magnetic anisotropy axes, which generate closed-loop toroidal magnetic moments decoupled from any primary magnetic direction.[8] This nonmagnetic ground state, ideally possessing zero net magnetic moment, renders SMTs inherently resistant to uniform magnetic fields. Additionally, the toroidal states can be modulated by the external electric field,[9] offering a viable solution for the read and write problems currently existing in electron spin-based molecular qubits. These combined properties make SMTs particularly attractive for applications in quantum sensing, molecular spintronics, and topologically protected qubit encoding.[10] However, controlling anisotropy axis orientation to stabilize toroidal states is highly nontrivial. Initially, toroidal moments were identified in planar $\{Dy_3\}$ triangles with in-plane magnetic axes,[6,11−13] but subsequent studies revealed that nonplanar geometries such as cubane-like $\{Dy_4\}$ can also host toroidal states.[14] Enhancing the stability and detectability of toroidal states requires careful molecular design (see Scheme 1).[15] Strategies include (i) increasing the number or spatial separation of spin centers, (ii) reinforcing dipolar and

Received: July 28, 2025
Revised: October 1, 2025
Accepted: October 1, 2025
Published: October 18, 2025

Scheme 1. Progress over the Years in Identifying SMT/FT Moments in the Ground State[a]

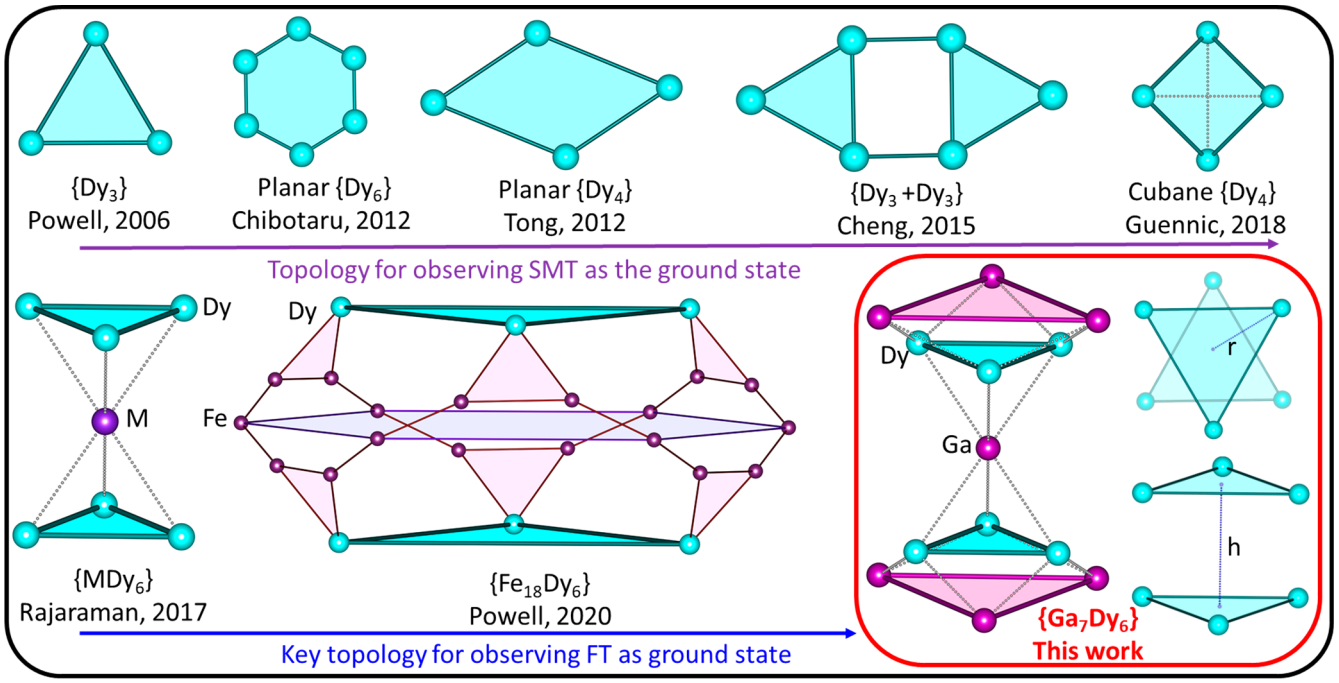

[a]The "h" and "r" in bottom right corner panel represent the centroid-to-centroid distance (h) between the {Dy_3} triangles and their radius (r).

exchange couplings, and (iii) exploiting the ferrotoroidal (FT) moment, in which the local magnetic moments circulate conrotatory, all clockwise or all anticlockwise, around the molecular core. This head-to-tail arrangement cancels the net magnetic moment, but the individual toroidal vectors add up, giving a nonzero net toroidal moment. By contrast, in an antiferrotoroidal (AFT) moment, neighboring toroidal units circulate in opposite senses, so their toroidal moments cancel each other.[9,16,17] A key challenge is maximizing the FT-AFT energy gap to protect the toroidal states from external perturbations. This gap is governed by the ratio between the centroid-to-centroid distance (h) of {Ln_3} triangles and their radius (r); a larger reduction in the h/r ratio enhances FT stabilization (see Scheme 1).[15,18] Accounting for an appropriate h/r ratio, the SMTs can exhibit enhanced slow magnetic relaxation that is distinct from conventional SMMs.[19] In addition to symmetry-imposed selection rules and the absence of net magnetization, many-body spin reversal is required, making quantum tunnelling energetically forbidden and drastically extending relaxation time scales.[20−22] Realizing such long-lived, magnetically silent states at the molecular level would be a major advance for QIS.

To this end, we have experimentally showcased the unprecedented slow relaxation of toroidal states in the molecular complex $[Ga_7Dy_6(N\text{-}mdea)_6(ClCH_2COO)_6(NO_3)_6(OH)_{12}(H_2O)_6]\cdot 3Cl$ (**1**). The unique arrangement of Ga(III) ions in **1** not only enhances magnetic anisotropy but also contributes to a reduced h/r ratio, a key parameter that dictates the FT-AFT gap. *Ab initio* CASSCF/RASSI-SO/SINGLE_ANISO/POLY_ANISO calculations suggest a vortex-like alignment of magnetic anisotropy axes, which is validated by μSQUID measurements, with an exceptionally slow relaxation time on the scale of ∼11 years, the longest ever reported for any MNMs, surpassing even the best Dy(III) SMMs reported to date. These findings demonstrate how topological design principles can yield robust, long-lived toroidal states, an observation with far-reaching implications for spin-based quantum technologies.

RESULT AND DISCUSSION

Synthesis, Structural Description, and Basic Magnetic Characterization. Complex **1** was synthesized by reacting $Ga(NO_3)_3\cdot xH_2O$, $Dy(NO_3)_3\cdot 6H_2O$, N-mdea, chloroacetic acid, and triethylamine in MeCN. The resulting gel-like mixture was redissolved in a 1:1 mixture of MeOH and ^{i}PrOH, and slow evaporation over 3−4 weeks yields colorless single crystals. The single crystal structure solution reveals the molecular formula $[Ga_7Dy_6(N\text{-}mdea)_6(ClCH_2COO)_6(NO_3)_6(OH)_{12}(H_2O)_6]\cdot 3Cl$ (**1**). Complex **1** crystallizes in the trigonal crystal system, $R\bar{3}$ space group (see Table S1). The detailed reaction scheme and structural description of **1** are provided in the Supporting Information text. Complex **1** possesses a unique metal core arrangement, where the hourglass {$GaDy_6$} core is sandwiched between two {Ga_3} triangles, forming a high-symmetry tridecanuclear assembly (see Figure 1a and Figure S1). Interionic separations are illustrated in the packing diagram (see Figure S2), and the geometry of individual Ga(III)/Dy(III) centers was further evaluated via shape analysis (see Table S2). Notably, the reduced {Dy_3−Dy_3} centroid-to-radius ratio in complex **1** (h/r = 2.375 Å), ∼0.2 Å shorter than in related systems, is expected to significantly influence dipolar interactions and promote the stabilization of toroidal states (see Table S3−S4 for selected bond lengths and angles).[15,23] The bulk phase purity was confirmed by powder X-ray diffraction prior to conducting direct current (DC) and alternating current (AC) magnetic susceptibility measurements (see Figure S3).

Variable-temperature DC magnetic susceptibility data (measured at 0.1 T) shows that a $\chi_m T$ value of 84.48 cm^3 K mol^{-1} at 300 K for **1** aligns well with the theoretically expected value for the six magnetically diluted Dy(III) ions (see Figure

https://doi.org/10.1021/jacs.5c12742
J. Am. Chem. Soc. 2025, 147, 39572−39581

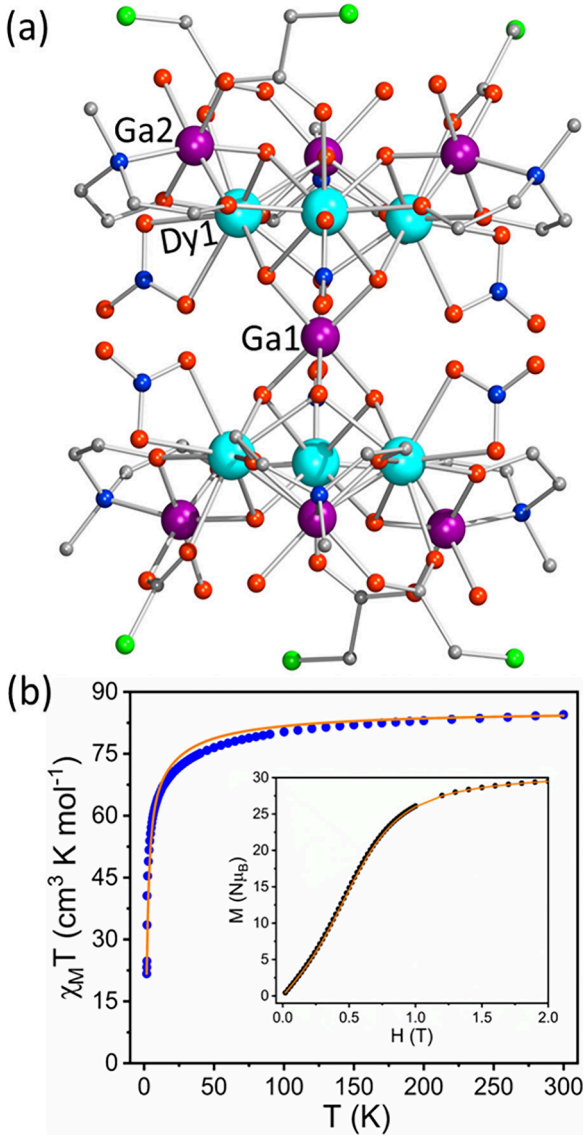

Figure 1. (a) Molecular crystal structure of the cationic core of complex **1** (color code: Ga(III), light violet; Dy(III), cyan; Cl, green; O, red; N, blue; C, gray). (b) DC magnetic susceptibility of complex **1**. Inset: Magnetization at 1.8 K was performed with experimental data (symbols) and computed values (solid orange line).

1b). With decreasing temperatures, the product of $\chi_m T$ gradually decreases to 75 K due to Stark sublevel depopulation, followed by a sharp decline to 20.5 cm^3 K mol^{-1} at 1.8 K, indicating dominant antiferromagnetic (AFM) interactions and magnetic anisotropy/dipolar coupling. The isothermal-field-dependent magnetization measurements show a gradual increase in magnetic moment and reach a final value of 32.08 Nμ_B at 1.8 K (7 T). This value is significantly smaller than the theoretically expected magnetic moment, indicative of strong magnetic anisotropy associated with Dy(III) ions in complex **1**. A careful analysis of the magnetization data for complex **1** reveals a characteristic low-field S-shaped curve (see Figure S4), indicative of SMT behavior (*vide infra*).[17,23,24]

AC susceptibility measurements performed on a polycrystalline sample of **1** reveal no out-of-phase (χ'') signal in the absence of a static DC magnetic field. However, upon applying an optimum DC field of 2400 Oe, frequency-dependent χ'' maxima emerge below ∼6 K (see Figure S5a-b), indicating field-induced SMM behavior. The Cole−Cole plots were fitted using the generalized Debye model to extract relaxation times (τ) and distribution parameters (α), revealing the presence of more than one relaxation process (Figure S5c). Fitting temperature-dependent relaxation times to the equation $\tau = \tau_0 \exp(U_{eff}/k_B T)$ yielded two Orbach-type processes, with effective energy barriers of U_{eff} = 8.29 ± 0.27 K (τ_0 = 5.2 × 10^{-8} s) and U_{eff} = 1.17 ± 0.03 K (τ_0 = 11.2 × 10^{-8} s), consistent with distinct quantum tunnelling regimes (see Figure S5d, Table S5−S6). A similar two-step relaxation behavior has been observed in related FT complexes.[25]

Theoretical Estimation of Ferrotoroidal-Antiferrotoroidal Gap and Toroidal Blocking. The triangular {Dy$_3$} units in **1** make it a suitable candidate for exploring the toroidal magnetic behavior. To investigate this and gain deeper insights into its electronic structure, we performed *ab initio* CASSCF/RASSI-SO/SINGLE_ANISO/POLY_ANISO calculations using the MOLCAS 8.2 suite (see computational details in Supporting Information).[12,26,27] Our investigation proceeded in three steps. First, we assessed the single-ion anisotropies of the six Dy(III) centers. Their calculated ground state Kramers doublet (KDs) g-tensors ($g_x \approx 0.105$, $g_y \approx 0.236$, $g_z \approx 19.616$) are similar to each other, which is not surprising considering the highly symmetric nature of **1** that exhibits pseudo-S6 symmetry. The computed g-tensors reveal the pronounced axial anisotropy, and the easy axes arrange in a vortex/circular pattern within each {Dy$_3$} triangle (see Figure 2), suggesting a

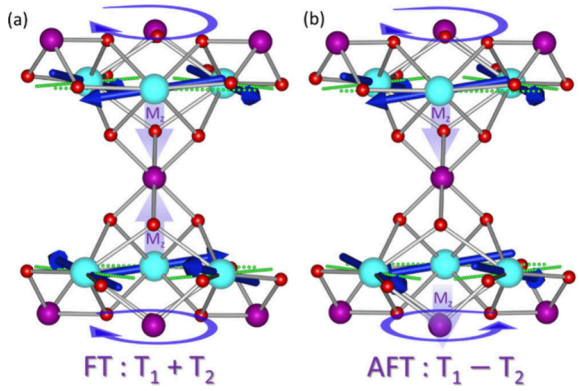

Figure 2. Orientation of the magnetic anisotropy axis: (a) FT configuration, with blue arrows on each Dy(III) center obtained from single-ion calculations and the parrot green line representing the ideal triangular tangent; (b) AFT configuration. The light violet arrow shows the magnetic moment along the z direction (M_z component) of each triangle.

toroidal ground state. This is consistent with the S-shaped magnetization curve observed for **1**. Further detailed analysis reveals that in both {Dy$_3$} triangles of **1**, the orientation of easy axes (head to tail) is arranged in the same direction, i.e., an FT scenario is witnessed in **1**. The energy gaps between the ground and first excited Kramers doublets span 68.1−69.6 cm^{-1}, and all Dy(III) centers display significant zero-field QTM in their single-ion analogue (see Figure S6 and Table S7). This is consistent with the rhombic g-tensors computed for these states. Clearly, the nonaxial crystal field parameters significantly contribute to the spin Hamiltonian, preventing zero-field SMM behavior (see Table S8).[28] This explains the absence of out-of-phase susceptibility signals when H_{DC} = 0 in **1**.

https://doi.org/10.1021/jacs.5c12742
J. Am. Chem. Soc. 2025, 147, 39572−39581

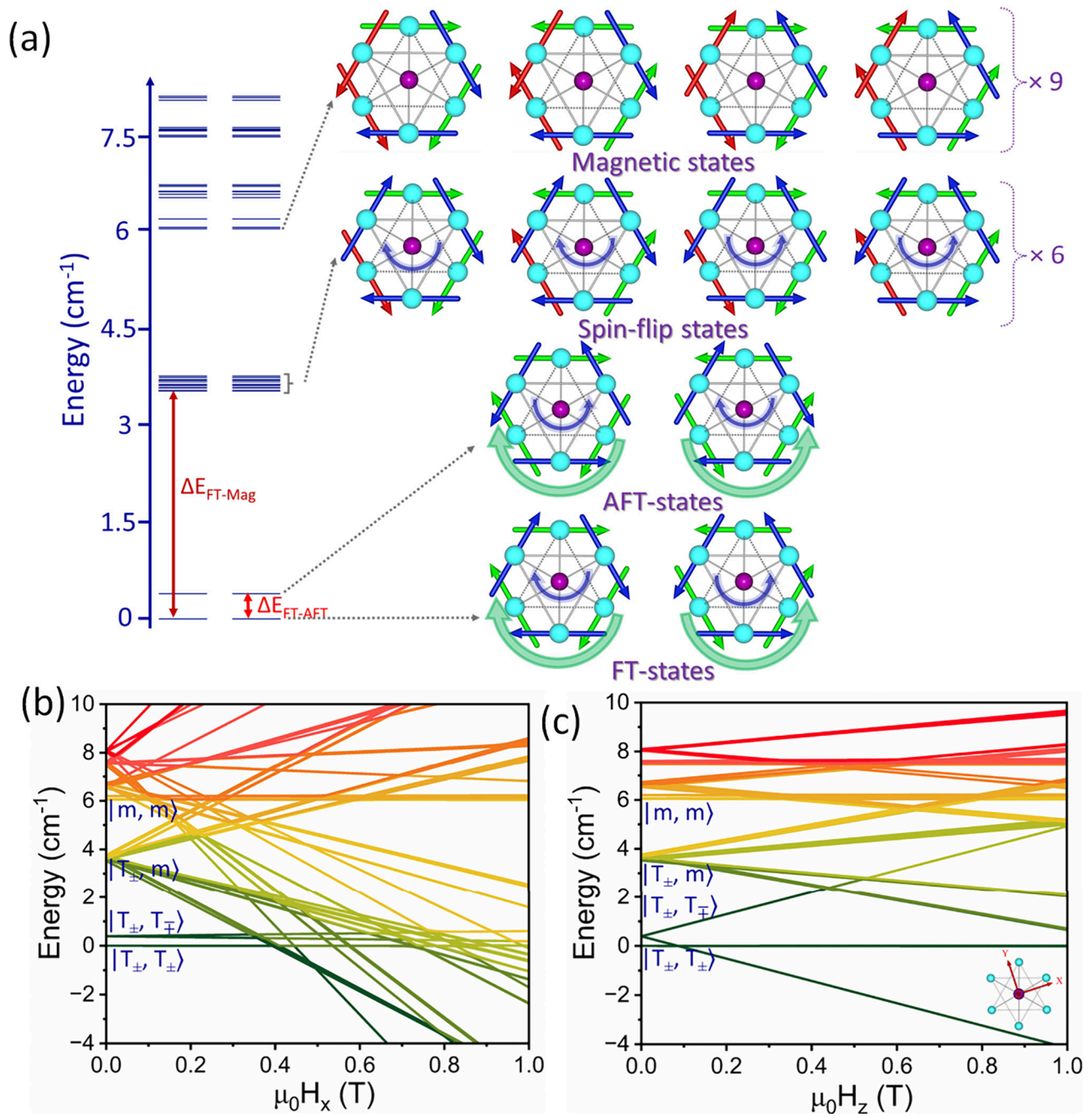

Figure 3. (a) Energy spectrum illustrating magnetic relaxation and toroidal states for complex **1**. The red double-headed arrow indicates the energy gap between the ground FT state $|\pm T_1, \pm T_2\rangle$ and the first excited AFT state $|\pm T_1, \mp T_2\rangle$. The brown double-headed arrow marks the energy separation between the FT state and the magnetic states ($\Delta E_{FT\text{-}Mag}$). (b) Computed Zeeman splitting diagram with the magnetic field applied along the *x*-axis; (c) the field applied along the *z*-axis.

Second, to evaluate the magnetic coupling between the Dy(III) ions and elucidate the energies of the exchange-coupled states in **1**, we employed the POLY_ANISO suite, using parameters extracted from SINGLE_ANISO calculations as input. POLY_ANISO uses the Lines model (S_i = 5/2) to incorporate exchange interactions (Equation S1) with user-inputs $J_{Lines,ex}$ for each pair, while pairwise on-site dipolar interactions ($J_{Ising,dip}$) are calculated (Equation S2,3) based on Dy(III) ions coordinates and easy-axis vectors. Note that interactions for all six Dy(III) ions (i.e., both intra- and intertriangular interactions) were incorporated.

As the dipolar interactions were fixed to their on-site calculated values, the exchange interactions needed to be estimated. For this purpose, the DFT calculations on an isostructural Gd(III)-based system were performed to get an initial guess of its order of magnitude (see supplementary text for more details). Eventually, their precise values were estimated based on the fitting of experimental DC susceptibility and magnetization data (see Figure 1b). The best fit yields isotropic intratriangular exchange $J^{intra}_{Lines,ex} = -0.030$ cm^{-1} and intertriangular exchange energy $J^{inter}_{Lines,ex} = -0.023$ cm^{-1}, while the dipolar interactions remain fixed to their on-site calculated values of the order: $J^{intra}_{Ising,dip} \approx -2.95$ cm^{-1} and $J^{inter}_{Ising,dip}$

https://doi.org/10.1021/jacs.5c12742
J. Am. Chem. Soc. 2025, 147, 39572−39581

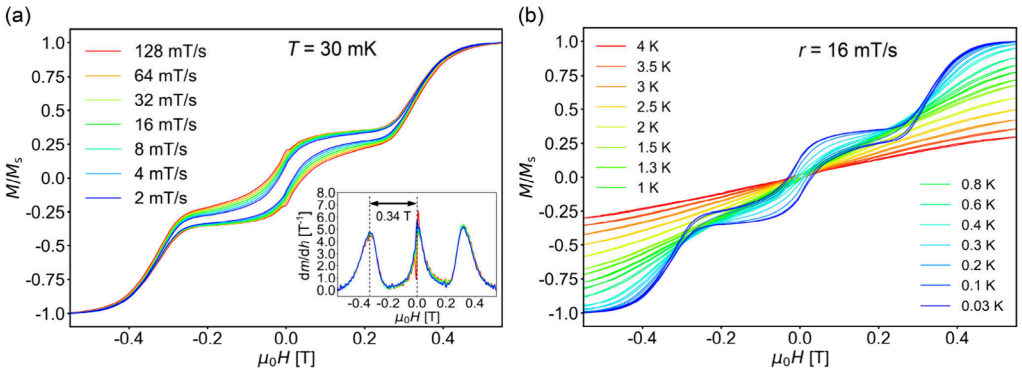

Figure 4. Magnetization vs field ($M(H)$) curves in a single crystal of complex **1** (crystal **#1**) measured by μSQUIDs. (a) at a fixed bath temperature T = 30 mK and different field sweep rates and (b) at a fixed field sweep rate = 16 mT/s and different bath temperatures. The inset shows the derivatives $dm/dh = \frac{1}{\mu_0 M_s} dM/dH$ corresponding to panel (a). The measurements are shown for a direction of the magnetic field closely aligned with an easy axis.

≈ -0.19 cm^{-1}. For a comparison between dipolar and exchange contributions, $J_{Lines,ex}$ were converted to their Ising analogue (see Equation S5) as $J^{intra}_{Ising,ex} = -0.38$ cm^{-1} and $J^{inter}_{Ising,ex} = -0.29$ cm^{-1}.

Importantly, the intratriangular coupling is the dominant contribution, as it governs the formation of the vortex arrangement. In contrast, the role of the small intertriangular interaction, consistent with the larger Dy···Dy separations between the two triangles (see Figure 1b, Figure S4), is primarily to split the FT and AFT states. The dominance of dipolar intratriangular interactions is evident, as verified by the fact that the low-temperature magnetization curves (see Figure S7) cannot be fitted without incorporating the dipolar contribution. However, the intertriangular exchange, being comparable to the intertriangular dipolar interaction, critically influences the FT-AFT gap.

Eventually, the inter- or intratriangular total interactions (exchange + dipolar) can be represented by $J_{Ising,total} = J_{Ising,ex} + J_{Ising,dip}$, or the corresponding total interaction ('-2J') between the actual moments ($m_{J,i} = 15/2$), related by $J_{Ising,total} \approx 450J \cos(60°)$ (Equation S4,5). The latter estimates $J = -0.015$ cm^{-1} (for intratriangular interaction) and $= -0.002$ cm^{-1} (for intertriangular interaction), with a reasonable agreement with the low-temperature measurements (*vide infra*).

Finally, we mapped the collective anisotropy of each Dy(III) ion in complex **1** to unambiguously establish the nature of the ground state. We found that each Dy(III) easy axis is canted by ~9° from its triangular plane (see Figure S8), and two competing states emerge. The ~9° canting arises from the off-plane μ_3-OH charges steering the Dy(III) anisotropy axes, modulated by subtle structural corrugation that mitigates the Dy···Dy dipolar interaction while maintaining the overall configuration. In the FT state, the individual toroidal moments with respect to center of mass ($T = \sum_{i=1}^{n} r_i \times S_i$ where r_i is the position vector of the i^{th} paramagnetic ion and the S_i is the local spin operator) of the two {Dy_3} units add, i.e. $T_{tot.} = T_1 + T_2$ where T_1 and T_2 are the toroidal moment from each {Dy_3} unit, while their z-components of magnetization cancel. The computed toroidal moment for each {Dy_3} is 67.94 μ_BÅ (see Figure S9; see supplementary text for more detail). In the AFT states, the toroidal moments cancel, i.e., $T_{tot.} = T_1 - T_2$, and the z-components of magnetization add up (~1 $g\mu_B m_J$). Crucially, the weak intertriangular exchange lifts the FT−AFT degeneracy by 0.39 cm^{-1}, cementing the FT state as the true ground state (see Figure 3; Figures S10−S11 show the degenerate situation in its absence). This FT−AFT gap is, to our knowledge, the largest yet reported for a discrete molecular complex (see Figure S12). This is enabled by high molecular symmetry and the incorporation of two diamagnetic {Ga_3} layers, which act as dielectric spacers while maintaining 6-fold symmetry, suppressing magnetic exchange and enhancing charge uniformity (the electric dipole moment is ~10-fold higher than in {$CrDy_6$}; Figure S13). As a result, complex **1** attains a truly nonmagnetic FT ground state, akin to the nonmagnetic state first observed in a planar {Dy_4} cluster, in contrast to the 3 μ_B plateau of {$CrDy_6$} or the residual 0.56 μ_B moment in the first reported {Dy_3} triangle.[8,13,17] Simulated Zeeman spectra further underscore this behavior and show directional sensitivity. With the field applied along x or y, FT and AFT states remain degenerate; along z, the AFT state splits owing to its tiny moment, whereas the FT state is immune (Figure S14). A spin-flip manifold appears from 3.52 to 3.76 cm^{-1} (24-fold degenerate), followed by additional magnetic states beyond 6.04 cm^{-1} (see Figure 3a). Two level crossings are predicted: one at 0.36 T between AFT and spin-flip states and another at 0.41 T between FT and spin-flip states (see Figure 3b). For magnetic fields in z-directed fields, FT remains degenerate, but the AFT states show significant splitting (Figure 3c). The lowest AFT tunnelling gap is only 4.4×10^{-16} cm^{-1} (see Tables S9−S10, Figure S15), implying exceptionally slow tunnelling and reinforcing the stability of the FT ground state. A preliminary comparison of the low-frequency modes between the {Dy_3}[29] and complex **1** was carried out through vibrational spectrum analysis (see Figure S16; supplementary text for more detail). Taken together, these calculations show how a high molecular symmetry, strategic diamagnetic spacing, and delicately balanced exchange interactions conspire to produce an unusually robust FT in complex **1**.

Toroidal State and Its Slow Relaxation Detected via μSQUID Measurements. *Dominant QTM Transitions in M(H) Loops at Sub-Kelvin Temperatures.* To investigate the toroidal ground states, we performed μSQUID magnetometry (see Supporting Information for details) down to a 30 mK temperature on single crystals of complex **1**. At 30 mK, the sweep rate-dependent $M(H)$ curves (see Figure 4a), for fields applied along a line of symmetry (see later) show a characteristic shape typical of triangular toroidal sys-

https://doi.org/10.1021/jacs.5c12742
J. Am. Chem. Soc. 2025, 147, 39572−39581

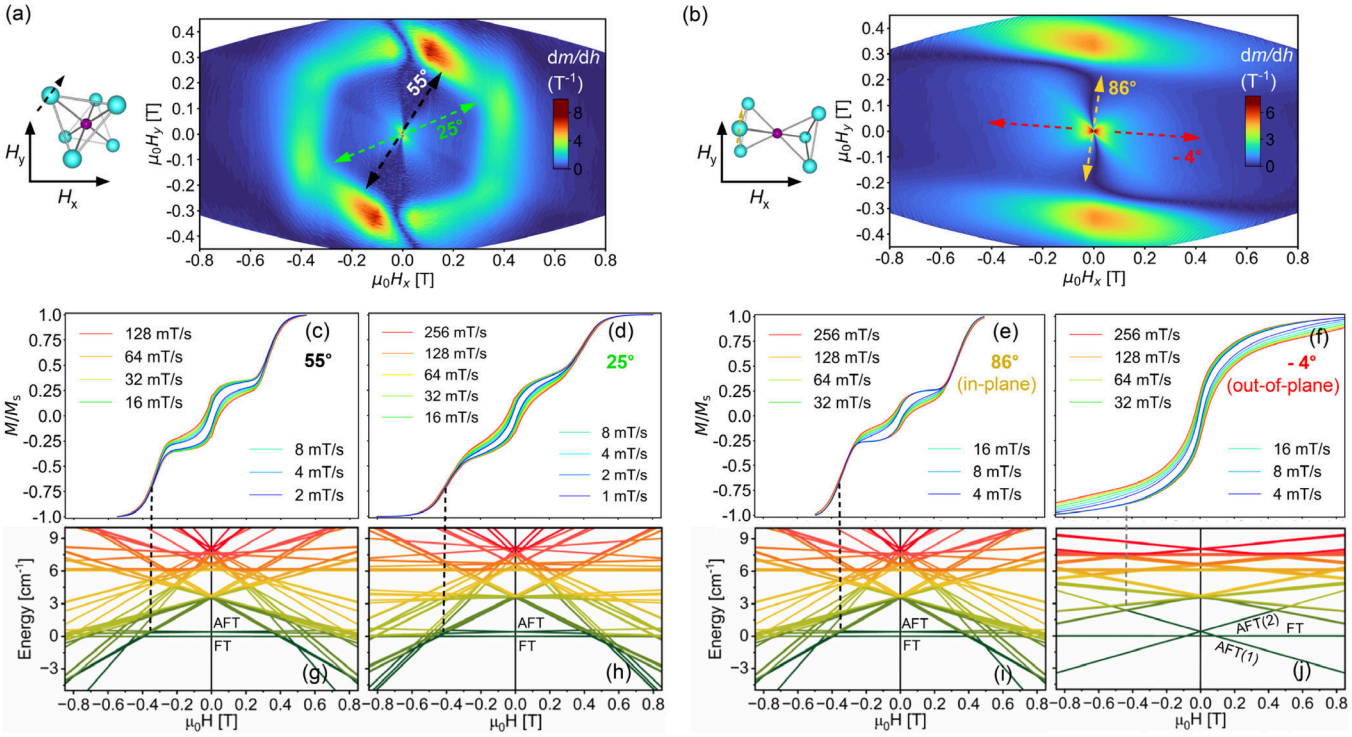

Figure 5. Derivative vs field-angle maps ($dm/dh(\theta)$), derived from angle-dependent $M(H)$ curves at T = 30 mK and r = 64 mT/s, are shown for two crystals (crystal **#1, #2**) of complex **1** in (a), (b) respectively. Crystal **#1** and **#2** were orientated differently in the μSQUID plane, with the estimated orientations of the molecule depicted on the left of each figure. The hexagonal shape in (a) indicates that the measurement plane was closely aligned with the Dy triangle plane for crystal **#1**, while crystal **#2** was placed with the Dy triangle plane perpendicular to the measurement plane according to panel (b). The sweep rate dependent $M(H)$ curves at 30 mK corresponding to two specific angles depicted in each derivative map are shown in (c)-(f) respectively. Simulated Zeeman diagrams that very closely correspond to each of these magnetic field directions are shown in (g)-(j).

tems.[15,17,30] A distinct step at ∼0.34 T indicates an antilevel crossing between an AFT and a spin-flip state, consistent with the Zeeman diagram (see Figure 3b). Although several additional crossings above 0.34 T are indicated in the Zeeman diagram, most of these are forbidden many-body cotunnelling, as detailed later. Temperature-dependent $M(H)$ curves (see Figure 4b) reveal that QTM steps smooth out and hysteresis diminishes above 1 K, suggesting enhanced underbarrier thermal relaxations.

At 30 mK, the prominent zero-field QTM transitions in the $M(H)$ loops suggest that a substantial fraction of molecules remains in excited states as the field is swept from saturation to zero. This excited-state population significantly contributes to the observed hysteresis but relaxes relatively quickly, resulting in sweep rate-dependent $M(H)$ curves (see Figure 4a) that apparently resemble those typically seen in other toroidal systems.[17]

However, an extremely slow relaxing component (i.e., a fraction of the population) was found to coexist, contributing subtly to the hysteresis, and could be isolated only via the long-waiting relaxation studies. In the following steps, we first present detailed angle-dependent $M(H)$ studies that directly confirm the toroidal ground state, followed by relaxation measurements to reveal and characterize the slow-relaxing component.

Confirming Toroidal Ground States by Angle-Dependent M(H). To confirm toroidal ground states and realize the intriguing contrast between the 'in-plane' (*x-y:* plane of the Dy(III) triangle) vs 'out-of-plane' (z) behavior anticipated from the Zeeman diagrams, we probe crystals from the same batch with two different orientations: the Dy(III) triangular plane (x-y) aligned with the μSQUID plane ($H_{x,y}$), and at 90° (i.e., the z axis lying in the $H_{x,y}$ plane). Figure 5a-b indicates the angular dependence in the $M(H)$ curves (at 30 mK) for these two cases, respectively, by plotting their derivatives $dm/dh = (1/\mu_0 M_s)dM/dH$ as a function of magnetic field direction (see the underlying $M(H)$ curves in Figures S17−S18).

The hexagonal-shaped anisotropy of the AFT to *spin-flip* transition (see Figure 5a) is ideally expected for fields varied *in-plane*, confirming a cyclic/toroidal arrangement. Each Dy(III) spin, with a ∼120° angle among its easy axes, can switch only along its respective easy directions due to the strongly dominating anisotropy, leading to three sets of parallel lines of a hexagon. The magnitude of the switching field ($\mu_0 H_{ex}$) depends on the effective interaction (J) at each site, as $\mu_0 H_{ex} = -2Jm_J/(g_J\mu_B)$[27] (see supplementary text for more detail). In this system, the bottom triangle is rotated by 60° with respect to the top, yielding another perfectly superposing hexagon. We note $\mu_0 H_{ex} \approx 0.34$ T, leading to $J \approx -0.014$ cm^{-1} in good agreement with the calculated total intratriangular interaction (*vide supra*).

For the external field along an easy axis, the $M(H)$ curves (see Figure 5c) show a flat region ($dm/dh \sim 0$) from −0.3 to 0 T, indicating the toroidal ground states with a negligible in-plane magnetic moment. The corresponding Zeeman diagram in Figure 5g, with fields along the in-plane projection of a Dy(III) easy axis, showed minimum Zeeman splitting of the AFT states, while the FT states remain completely degenerate. While for the external field along a corner of the anisotropy-hexagon, the $M(H)$ curves (see Figure 5d) show a 'sickle'

https://doi.org/10.1021/jacs.5c12742
J. Am. Chem. Soc. 2025, 147, 39572−39581

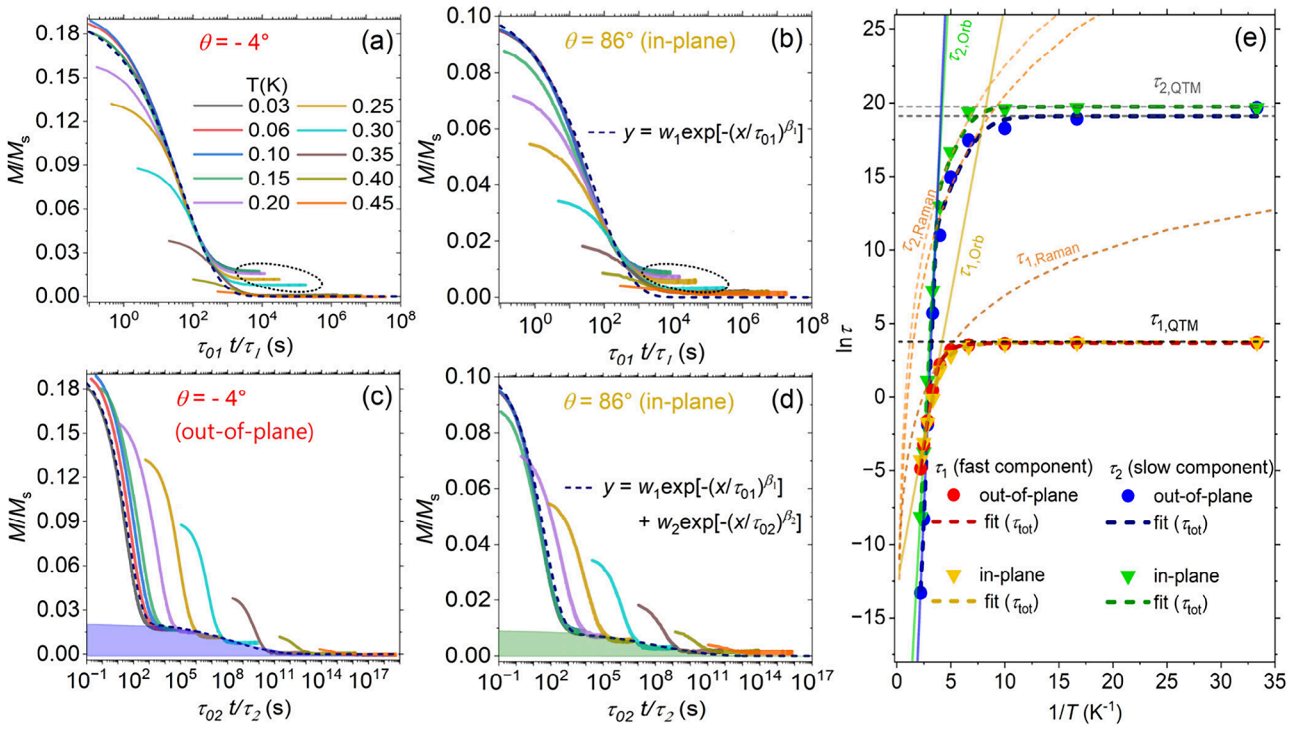

Figure 6. Magnetization relaxation curves obtained after a field sweep from saturation field to zero, measured in crystal **#2** at different bath temperatures. The magnetic field direction was fixed to two specific directions within the μSQUID plane, as depicted in Figure 5. The raw data (SI) at each temperature was scaled with a factor in the x axis to obtain a master curve. Panels (a), (b) show the scaled relaxation curves for the two angles respectively, where the relaxation times are scaled to obtain a master curve for only the fast-relaxing components (fitted dashed line). Panels (c), (d) show the scaled relaxation curves for the slow relaxing components, yielding a master curve that contains both relaxation times (fitted dashed line). These yield two relaxation times for each angle as plotted in (e) as a function of $1/T$.

shape with nonzero dm/dh throughout the relevant region. It is possibly a signature of the slow-relaxing AFT states that undergo small Zeeman splitting when the field is not aligned with an easy axis.

The presence of the AFT states is further revealed in the second kind of angular map with the 'z' axis of the molecule within the measurement plane (see Figure 5b). Intriguingly, the shape of the $M(H)$ curve changes drastically as the field direction varies from *in-plane* (see Figure 5e) to *out-of-plane* (see Figure 5f) of the Dy(III) triangle, with the latter showing a large transition near the zero field as the other two transitions moved toward infinite fields (see Figure S16). The signal strength ($\sim M$) in the μSQUID measurements did not significantly reduce between Figure 5e-f, confirming that six Dy(III) spins of an AFT state (each at +9.4° angle out of the triangle-plane) add up to $6g\mu_B m_J \sin(9.4°) \sim 0.97 g\mu_B m_J$ *out-of-plane* moment, comparable to the *in-plane* magnetic moment of a single-spin-flip state. The same can be realized by comparing the Zeeman diagrams and those computed from the *ab initio* calculation (see the above section and Figure 5i-j): the slope of the spin-flip states in Figure 5i is comparable to the slope of the AFT states in Figure 5j. Notice that the dominant magnetic part in Figure 5j is the AFT states, and in this case, the crossing between the lower AFT and the lowest spin flip states moved out of the maximum field range to infinity. Hence, the $M(H)$ loops in Figure 5f should bear an enhanced signature of the AFT states' relaxation.

Isolation of the Slow-Relaxing Components by Magnetic Relaxation Measurements. The presence of AFT states is indicated; however, the isolation of FT states remains challenging, as the relaxation between the Zeeman-split AFT states and the relaxation from AFT to an FT state are both slow and indistinguishable. The zero-field QTM paths for these states are mostly forbidden, while those for the excited-state population are relatively probable. To extend this argument further, the Zeeman diagrams show many crossings, but QTM practically happens only at the crossings that involve one- or two spin-flip events. An earlier study on a similar system[17] utilized density matrix calculations to fit $M(H)$ curves and yield individual tunnel rates. It showed that one- and two-body tunnelling rates are significantly higher than many spin-flip cotunnelling events, as observed in other molecular magnets.[20,31] The zero-field QTM between the two Zeeman split AFT states, and the QTM between an AFT and FT state in Figure 5j are six-body and three-body tunneling processes, respectively, hence mostly quenched.

Hence, a part of the population (spin-flip states) should relax fast (via two-body tunneling and enhanced thermal pathways), while the rest remaining in the AFT states should show slower relaxation. Additionally, Figure 5j showed that spin-flip states do not intersect the lower AFT state, implying a likely increase in the initial AFT population for *out-of-plane* measurement. To investigate these aspects, we measured temperature-dependent magnetization relaxation ($M(t)$) curves in crystal #2 for magnetic fields in *in-plane* (see Figure S19b) and *out-of-plane* (see Figure S19a) directions, i.e., along the two arrows in Figure 5(b). Multiple parallel and serial relaxation pathways can lead to significant deviation from a stretched exponential relaxation curve;[32] hence, scaling to a master curve (see Figure 6a-b) is usually a more generic way to obtain temperature-dependent mean relaxation times. In Figure 6a-b, the master curve that considers only one mean-

https://doi.org/10.1021/jacs.5c12742
J. Am. Chem. Soc. 2025, 147, 39572−39581

relaxation time, i.e. $M(t) = M_0 e^{-(t/\tau_{01})\beta_1}$ with $\tau_{01} \approx 45$ s, clearly does not capture the fraction that relaxes extremely slowly (see circular mark in Figure 6a-b or large time region in Figures S19a-b). To reconcile this information, the $M(t)$ curves were rescaled to the master curve that captures both the relaxation time scales, see Figure 6c-d. A simulation with a double stretched exponential $M(t) = M_0 [w_1 e^{-(t/\tau_{01})\beta_1} + w_2 e^{-(t/\tau_{02})\beta_2}]$ yields $\tau_{01} \approx 41$ s and $\tau_{02} \approx 3.5 \times 10^8$ s (for both *out-of-plane* and *in-plane* directions, see Figure 6c,d), i.e. two time scales separated by several decades on the log scale.. A difference was found in their relative weights by comparing in-plane and out-of-plane directions (see supplementary text for more detail), consistent with AFT states being the slow-relaxing component. Interestingly, the low-temperature relaxation time of the slow components ($\tau_{02} \approx 11$ years) counts among the largest quantum tunnelling times reported in any single molecule magnet (see Table S11).[20,22,27]

Finally, Figure 6e shows the obtained relaxation times $\tau_{1,2}$, from the individual scaling, plotted as a function of $1/T$ and fitted considering an Orbach, a Raman, and a QTM time scale[27] as $\ln(\tau) = -\ln[\tau_0^{-1}\exp(-U_{eff}/k_BT) + CT^n + 1/\tau_Q]$ (see supplementary text for more detail). Due to the missing high temperature part, these fittings cannot be completely rationalized.[27] Rather, an effective barrier U_{eff} can be estimated by assuming Arrhenius-like behavior (an Orbach process) at $T > 300$ mK, to compare the fast and slow relaxing components at higher temperatures. The obtained U_{eff} were ~14 K for the slow components and ~3.5 K for the fast components, indicating that both QTM time and thermal relaxation times are larger for the toroidal states. Notably, these effective barriers are comparable to the energy gaps between the *toroidal states* (or *spin-flip* states, respectively) and the cluster of *magnetic states* located at the top of the Zeeman diagrams shown in Figure 5. This suggests that a thermal relaxation pathway from one chirality (or spin-flip orientation) to the other is via the *magnetic states*.

CONCLUSIONS

Quantum information science (QIS) demands molecular systems that offer long coherence times and tunable quantum states, requirements that toroidal magnetic states are uniquely suited to meet, owing to their magnetic silence, robustness against uniform magnetic fields, and potential for electric-field-driven chiral control. Yet, realizing slow-relaxing ferrotoroidal (FT) ground states remains a significant synthetic and conceptual challenge. In particular, achieving nonmagnetic FT states with sizable FT−AFT energy gaps through the coupling of multiple toroidal $\{Dy_3\}$ units has proven especially elusive. In this work, we present the synthesis and full characterization of a tridecanuclear heterobimetallic cluster, $[Ga_7Dy_6(N\text{-mdea})_6(ClCH_2COO)_6(NO_3)_6(OH)_{12}(H_2O)_6]\cdot 3Cl$ (**1**), where the $\{GaDy_6\}$ core adopts an hourglass-shaped architecture, and the flanking $\{Ga_3\}$ triangles act as diamagnetic dielectric layers. This structural motif stabilizes the FT ground state and yields a record-high FT−AFT gap of ~0.4 cm^{-1} by effectively tuning the h/r ratio. *Ab initio* CASSCF calculations, static/dynamic magnetic data, and single-crystal micro-SQUID measurements confirm the FT ground state, marked by a distinct hexagonal in-plane anisotropy. Complex **1** exhibits a fractional population with quantum tunnelling of magnetization (QTM) relaxation time of $\sim 3.5 \times 10^8$ s (~11 years), among the slowest reported in molecular magnets. This ultraslow relaxation arises due to the quenched many-body tunneling between the AFT states and AFT to the nonmagnetic FT states. This work provides a clear molecular design blueprint for achieving robust and long-lived toroidal states, an essential step toward realizing coherent, magnetically silent, and stable spin architectures for QIS. Future molecular designs will focus on quenching spin-flip tunneling through the introduction of additional exchange bias, thereby favoring full population of the toroidal ground state and further extending QTM times. Combining this approach with strategies to enhance blocking temperatures could lead to significant advancements in the single-molecule magnet performance.

ASSOCIATED CONTENT

Supporting Information

The Supporting Information is available free of charge at https://pubs.acs.org/doi/10.1021/jacs.5c12742.

> The experimental, crystallographic, and computational details include SQUID instrumentation for magnetic measurements, with recorded data and plots for magnetization vs temperature and field; additionally, *ab initio* calculations were performed to investigate the magnetic properties of individual Dy sites and the low-lying spectrum of magnetic states in the complex **1**, directional dependent Zeeman spectrum, a comparison of presence and the absence of intertriangular dipolar coupling (PDF)

Accession Codes

Deposition Number 2475930 contains the supplementary crystallographic data for this paper. These data can be obtained free of charge via the joint Cambridge Crystallographic Data Centre (CCDC) and Fachinformationszentrum Karlsruhe Access Structures service.

AUTHOR INFORMATION

Corresponding Authors

Sagar Paul − *Physikalisches Institut, Karlsruhe Institute of Technology (KIT), D-76131 Karlsruhe, Germany;* orcid.org/0000-0001-8317-5778; Email: sagar.paul@kit.edu

Wolfgang Wernsdorfer − *Physikalisches Institut, Karlsruhe Institute of Technology (KIT), D-76131 Karlsruhe, Germany; Institute of Quantum Materials and Technologies (IQMT), Karlsruhe Institute of Technology (KIT), D-76344 Eggenstein-Leopoldshafen, Germany;* orcid.org/0000-0003-4602-5257; Email: wolfgang.wernsdorfer@kit.edu

Maheswaran Shanmugam − *Department of Chemistry, Indian Institute of Technology Bombay, Mumbai 400076 Maharashtra, India;* orcid.org/0000-0002-9012-743X; Email: eswar@chem.iitb.ac.in

Gopalan Rajaraman − *Department of Chemistry, Indian Institute of Technology Bombay, Mumbai 400076 Maharashtra, India;* orcid.org/0000-0001-6133-3026; Email: rajaraman@chem.iitb.ac.in

Authors

Deepanshu Chauhan − *Department of Chemistry, Indian Institute of Technology Bombay, Mumbai 400076 Maharashtra, India*

Dipanti Borah − *Department of Chemistry, Indian Institute of Technology Bombay, Mumbai 400076 Maharashtra, India*

https://doi.org/10.1021/jacs.5c12742
J. Am. Chem. Soc. 2025, 147, 39572−39581

Appu Sunil − *Physikalisches Institut, Karlsruhe Institute of Technology (KIT), D-76131 Karlsruhe, Germany*

Complete contact information is available at: https://pubs.acs.org/10.1021/jacs.5c12742

Notes

The authors declare no competing financial interest.

■ ACKNOWLEDGMENTS

The authors express gratitude to various funding agencies for their financial support. G.R. extends thanks to DST and SERB for funding, with Grant Nos. SB/SJF/2019-20/12 and CRG/2022/001697. G.R. acknowledge funding support from the National Quantum Mission (DST/QTC/NQM/QMD/2024/4), an initiative of the Department of Science and Technology, Government of India. M.S. extends thanks to BRNS (Grant No. 58/14/07/2023-BRNS/37029), CSIR (Grant No. 01(2933)/18/EMR-II), SERB (CRG/2023/002178), IISc-STARs (MoE-STARS/STARS-2/2023-0158), and IIT Bombay. W.W. thanks the German research foundation (DFG) for the Gottfried Wilhelm Leibniz-Award, ZVN-2020_WE 4458_5. D.C. is thankful to the University Grant Commission, and D.B. thanks CSIR for the graduate fellowship.

■ REFERENCES

(1) (a) Shiddiq, M.; Komijani, D.; Duan, Y.; Gaita-Ariño, A.; Coronado, E.; Hill, S. Enhancing coherence in molecular spin qubits via atomic clock transitions. *Nature* **2016**, *531* (7594), 348−351. (b) Gaita-Ariño, A.; Luis, F.; Hill, S.; Coronado, E. Molecular spins for quantum computation. *Nat. Chem.* **2019**, *11* (4), 301−309. (c) Moreno-Pineda, E.; Wernsdorfer, W. Measuring molecular magnets for quantum technologies. *Nat. Rev. Phys.* **2021**, *3* (9), 645−659. (d) Atzori, M.; Sessoli, R. The second quantum revolution: role and challenges of molecular chemistry. *J. Am. Chem. Soc.* **2019**, *141* (29), 11339−11352. (e) Wasielewski, M. R.; Forbes, M. D.; Frank, N. L.; Kowalski, K.; Scholes, G. D.; Yuen-Zhou, J.; Baldo, M. A.; Freedman, D. E.; Goldsmith, R. H.; Goodson, T., III; et al. Exploiting chemistry and molecular systems for quantum information science. *Nat. Rev. Chem.* **2020**, *4* (9), 490−504.

(2) Goodwin, C. A.; Ortu, F.; Reta, D.; Chilton, N. F.; Mills, D. P. Molecular magnetic hysteresis at 60 K in dysprosocenium. *Nature* **2017**, *548* (7668), 439−442.

(3) Woodruff, D. N.; Winpenny, R. E.; Layfield, R. A. Lanthanide single-molecule magnets. *Chem. Rev.* **2013**, *113* (7), 5110−5148.

(4) (a) Gould, C. A.; McClain, K. R.; Reta, D.; Kragskow, J. G.; Marchiori, D. A.; Lachman, E.; Choi, E.-S.; Analytis, J. G.; Britt, R. D.; Chilton, N. F.; et al. Ultrahard magnetism from mixed-valence dilanthanide complexes with metal-metal bonding. *Science* **2022**, *375* (6577), 198−202. (b) Guo, F.-S.; Day, B. M.; Chen, Y.-C.; Tong, M.-L.; Mansikkamäki, A.; Layfield, R. A. Magnetic hysteresis up to 80 K in a dysprosium metallocene single-molecule magnet. *Science* **2018**, *362* (6421), 1400−1403.

(5) (a) Swain, A.; Sharma, T.; Rajaraman, G. Strategies to quench quantum tunneling of magnetization in lanthanide single molecule magnets. *Chem. Commun.* **2023**, *59* (22), 3206−3228. (b) Bogani, L.; Wernsdorfer, W. Molecular spintronics using single-molecule magnets. *Nat. Mater.* **2008**, *7* (3), 179−186. (c) Chauhan, D.; Tiwari, R. K.; Rajaraman, G. Surface Stabilization to Enhance Single Molecule Toroidal Behavior in {Dy3} Molecules: the Impact of Au (111), MgO, and Graphene Surfaces. *Small* **2025**, *21* (11), No. 2412283.

(6) Li, X.-L.; Tang, J. Recent developments in single-molecule toroics. *Dalton Trans.* **2019**, *48* (41), 15358−15370.

(7) Chauhan, D.; Vignesh, K. R.; Swain, A.; Langley, S. K.; Murray, K. S.; Shanmugam, M.; Rajaraman, G. Exploiting Strong {CrIII−DyIII} Ferromagnetic Exchange Coupling to Quench Quantum Tunneling of Magnetization in a Novel {CrIII2DyIII3} Single-Molecule Magnet. *Cryst. Growth Des.* **2023**, *23* (1), 197−206.

(8) Chibotaru, L.; Ungur, L.; Soncini, A. The origin of non-magnetic Kramers doublets in the ground state of dysprosium triangles: evidence for a toroidal magnetic moment. *Angew. Chem., Int. Ed.* **2008**, *47* (22), 4126−4129.

(9) Zimmermann, A. S.; Meier, D.; Fiebig, M. Ferroic nature of magnetic toroidal order. *Nat. Commun.* **2014**, *5* (1), 4796.

(10) (a) Soncini, A.; Chibotaru, L. F. Toroidal magnetic states in molecular wheels: Interplay between isotropic exchange interactions and local magnetic anisotropy. *Phys. Rev. B Condens.* **2008**, *77* (22), No. 220406. (b) Pavlyukh, Y. Toroidal spin states in molecular magnets. *Phys. Rev. B* **2020**, *101* (14), No. 144408. (c) Luzon, J.; Bernot, K.; Hewitt, I. J.; Anson, C. E.; Powell, A. K.; Sessoli, R. Spin Chirality in a Molecular Dysprosium Triangle:<? format?> The Archetype of the Noncollinear Ising Model. *Phys. Rev. Lett.* **2008**, *100* (24), No. 247205. (d) Hymas, K.; Soncini, A.; Vignesh, K. R.; Chauhan, D.; Swain, A.; Benjamin, S. L.; Borah, D.; Shanmugam, M.; Wernsdorfer, W.; Rajaraman, G.; et al. Discriminating ferrotoroidic from antiferrotoroidic ground states using a 3d quantum spin sensor. *npj Quantum Mater.* **2024**, *9* (1), 106. (e) Popov, A.; Plokhov, D.; Zvezdin, A. Magnetoelectricity of single molecular toroics: The Dy 4 ring cluster. *Phys. Rev. B* **2016**, *94* (18), No. 184408.

(11) (a) Spaldin, N. A.; Fiebig, M.; Mostovoy, M. The toroidal moment in condensed-matter physics and its relation to the magnetoelectriceffect. *J. Phys.: Condens. Matter* **2008**, *20* (43), No. 434203. (b) Li, X. L.; Ma, Z.; Tang, J. Recent Developments of Nontraditional Single-Molecule Toroics. *Chem. Eur. J.* **2024**, *30* (27), No. e202304369. (c) Yang, Q.; Ungur, L.; Chibotaru, L. F.; Tang, J. Toroidal versus centripetal arrangement of the magnetic moment in a Dy4 tetrahedron. *Chem. Commun.* **2022**, *58* (11), 1784−1787. (d) Lin, S. Y.; Wernsdorfer, W.; Ungur, L.; Powell, A. K.; Guo, Y. N.; Tang, J.; Zhao, L.; Chibotaru, L. F.; Zhang, H. J. Coupling Dy3 triangles to maximize the toroidal moment. *Angew. Chem., Int. Ed.* **2012**, *51* (51), 12767−12771. (e) Li, X.-L.; Wu, J.; Tang, J.; Le Guennic, B.; Shi, W.; Cheng, P. A planar triangular Dy 3+ Dy 3 single-molecule magnet with a toroidal magnetic moment. *Chem. Commun.* **2016**, *52* (61), 9570−9573. (f) Ungur, L.; Langley, S. K.; Hooper, T. N.; Moubaraki, B.; Brechin, E. K.; Murray, K. S.; Chibotaru, L. F. Net toroidal magnetic moment in the ground state of a {Dy6}-triethanolamine ring. *J. Am. Chem. Soc.* **2012**, *134* (45), 18554−18557. (g) Lu, J.; Montigaud, V.; Cador, O.; Wu, J.; Zhao, L.; Li, X.-L.; Guo, M.; Le Guennic, B.; Tang, J. Lanthanide (III) hexanuclear circular helicates: slow magnetic relaxation, toroidal arrangement of magnetic moments, and magnetocaloric effects. *Inorg. Chem.* **2019**, *58* (18), 11903−11911. (h) Wu, J.; Li, X.-L.; Guo, M.; Zhao, L.; Zhang, Y.-Q.; Tang, J. Realization of toroidal magnetic moments in heterometallic 3d−4f metallocycles. *Chem. Commun.* **2018**, *54* (9), 1065−1068. (i) Mondal, S.; Chauhan, D.; Guizouarn, T.; Pointillart, F.; Rajaraman, G.; Steiner, A.; Baskar, V. Self-Assembled Lanthanide Phosphinate Square Grids (Ln= Er, Dy, and Tb): Dy4 Shows SMM/SMT and Tb4 SMT Behavior. *Inorg. Chem.* **2024**, *63* (47), 22338−22348.

(12) Zhang, H.-L.; Zhai, Y.-Q.; Qin, L.; Ungur, L.; Nojiri, H.; Zheng, Y.-Z. Single-molecule toroic design through magnetic exchange coupling. *Matter* **2020**, *2* (6), 1481−1493.

(13) Guo, P.-H.; Liu, J.-L.; Zhang, Z.-M.; Ungur, L.; Chibotaru, L. F.; Leng, J.-D.; Guo, F.-S.; Tong, M.-L. The first {Dy4} single-molecule magnet with a toroidal magnetic moment in the ground state. *Inorg. Chem.* **2012**, *51* (3), 1233−1235.

(14) (a) Fernandez Garcia, G.; Guettas, D.; Montigaud, V.; Larini, P.; Sessoli, R.; Totti, F.; Cador, O.; Pilet, G.; Le Guennic, B. A Dy4 Cubane: A New Member in the Single-Molecule Toroics Family. *Angew. Chem., Int. Ed.* **2018**, *130* (52), 17335−17339. (b) Das, C.; Vaidya, S.; Gupta, T.; Frost, J. M.; Righi, M.; Brechin, E. K.; Affronte, M.; Rajaraman, G.; Shanmugam, M. Single-Molecule Magnetism, Enhanced Magnetocaloric Effect, and Toroidal Magnetic Moments in a Family of Ln4 Squares. *Chem. Eur. J.* **2015**, *21* (44), 15639−15650.

(15) Murray, K. *Single molecule toroics: Synthetic strategies, theory and applications*; Springer, 2022.
(16) (a) Ding, L.; Xu, X.; Jeschke, H. O.; Bai, X.; Feng, E.; Alemayehu, A. S.; Kim, J.; Huang, F.-T.; Zhang, Q.; Ding, X.; et al. Field-tunable toroidal moment in a chiral-lattice magnet. *Nat. Commun.* **2021**, *12* (1), 5339. (b) Baum, M.; Schmalzl, K.; Steffens, P.; Hiess, A.; Regnault, L.; Meven, M.; Becker, P.; Bohatý, L.; Braden, M. Controlling toroidal moments by crossed electric and magnetic fields. *Phys. Rev. B Condens.* **2013**, *88* (2), No. 024414. (c) Gnewuch, S.; Rodriguez, E. E. The fourth ferroic order: Current status on ferrotoroidic materials. *J. Solid State Chem.* **2019**, *271*, 175−190. (d) Kaemmerer, H.; Baniodeh, A.; Peng, Y.; Moreno-Pineda, E.; Schulze, M.; Anson, C. E.; Wernsdorfer, W.; Schnack, J. r.; Powell, A. K. Inorganic approach to stabilizing nanoscale toroidicity in a tetraicosanuclear Fe18Dy6 single molecule magnet. *J. Am. Chem. Soc.* **2020**, *142* (35), 14838−14842.
(17) Vignesh, K. R.; Soncini, A.; Langley, S. K.; Wernsdorfer, W.; Murray, K. S.; Rajaraman, G. Ferrotoroidic ground state in a heterometallic {CrIIIDyIII6} complex displaying slow magnetic relaxation. *Nat. Commun.* **2017**, *8* (1), 1023.
(18) Ashtree, J. M.; Borilović, I.; Vignesh, K. R.; Swain, A.; Hamilton, S. H.; Whyatt, Y. L.; Benjamin, S. L.; Phonsri, W.; Forsyth, C. M.; Wernsdorfer, W.; et al. Tuning the Ferrotoroidic Coupling and Magnetic Hysteresis in Double-Triangle Complexes {Dy3MIIIDy3} via the MIII-linker. *Eur. J. Inorg. Chem.* **2021**, *2021* (5), 435−444.
(19) Zabala-Lekuona, A.; Seco, J. M.; Colacio, E. Single-Molecule Magnets: From Mn12-ac to dysprosium metallocenes, a travel in time. *Coord. Chem. Rev.* **2021**, *441*, No. 213984.
(20) Wernsdorfer, W.; Bhaduri, S.; Tiron, R.; Hendrickson, D.; Christou, G. Spin-spin cross relaxation in single-molecule magnets. *Phys. Rev. Lett.* **2002**, *89* (19), No. 197201.
(21) (a) Wernsdorfer, W.; Bhaduri, S.; Vinslava, A.; Christou, G. Landau-Zener tunneling in the presence of weak intermolecular interactions in a crystal of Mn 4 single-molecule magnets. *Phys. Rev. B Condens.* **2005**, *72* (21), No. 214429. (b) Hymas, K.; Soncini, A. The Role of Magnetic Dipole—Dipole Coupling in Quantum Single-Molecule Toroics. *Magnetochemistry* **2022**, *8* (5), 58.
(22) Soler, M.; Wernsdorfer, W.; Abboud, K. A.; Huffman, J. C.; Davidson, E. R.; Hendrickson, D. N.; Christou, G. Single-molecule magnets: two-electron reduced version of a Mn12 complex and environmental influences on the magnetization relaxation of (PPh4) 2 [Mn12O12 (O2CCHCl2) 16 (H2O) 4]. *J. Am. Chem. Soc.* **2003**, *125* (12), 3576−3588.
(23) Novitchi, G.; Pilet, G.; Ungur, L.; Moshchalkov, V. V.; Wernsdorfer, W.; Chibotaru, L. F.; Luneau, D.; Powell, A. K. Heterometallic Cu II/Dy III 1D chiral polymers: chirogenesis and exchange coupling of toroidal moments in trinuclear Dy 3 single molecule magnets. *Chem. Sci.* **2012**, 3 (4), 1169−1176.
(24) Chilton, N. F.; Anderson, R. P.; Turner, L. D.; Soncini, A.; Murray, K. S. PHI: A powerful new program for the analysis of anisotropic monomeric and exchange-coupled polynuclear d-and f-block complexes. *J. Comput. Chem.* **2013**, *34* (13), 1164−1175.
(25) Vignesh, K. R.; Langley, S. K.; Swain, A.; Moubaraki, B.; Damjanović, M.; Wernsdorfer, W.; Rajaraman, G.; Murray, K. S. Slow Magnetic Relaxation and Single-Molecule Toroidal Behaviour in a Family of Heptanuclear {CrIIILnIII6}(Ln= Tb, Ho, Er) Complexes. *Angew. Chem., Int. Ed.* **2018**, *130* (3), 787−792.
(26) (b) Ungur, L.; Van den Heuvel, W.; Chibotaru, L. F. Ab initio investigation of the non-collinear magnetic structure and the lowest magnetic excitations in dysprosium triangles. *New J. Chem.* **2009**, *33* (6), 1224−1230. (a) Aquilante, F.; Autschbach, J.; Carlson, R. K.; Chibotaru, L. F.; Delcey, M. G.; De Vico, L.; Fdez. Galván, I.; Ferré, N.; Frutos, L. M.; Gagliardi, L. Molcas 8: New capabilities for multiconfigurational quantum chemical calculations across the periodic table. *J. Comp. Chem* **2016**, *37* (5), 506.
(27) Zhu, Z.; Paul, S.; Zhao, C.; Wu, J.; Ying, X.; Ungur, L.; Wernsdorfer, W.; Meyer, F.; Tang, J. Record quantum tunneling time in an air-stable exchange-bias dysprosium macrocycle. *J. Am. Chem. Soc.* **2024**, *146* (28), 18899−18904.
(28) (a) Canaj, A. B.; Dey, S.; Martí, E. R.; Wilson, C.; Rajaraman, G.; Murrie, M. Insight into D6h Symmetry: Targeting Strong Axiality in Stable Dysprosium (III) Hexagonal Bipyramidal Single-Ion Magnets. *Angew. Chem., Int. Ed.* **2019**, *58* (40), 14146−14151. (b) Gupta, S. K.; Rajeshkumar, T.; Rajaraman, G.; Murugavel, R. An air-stable Dy (III) single-ion magnet with high anisotropy barrier and blocking temperature. *Chem. Sci.* **2016**, *7* (8), 5181−5191.
(29) Tang, J.; Hewitt, I.; Madhu, N.; Chastanet, G.; Wernsdorfer, W.; Anson, C. E.; Benelli, C.; Sessoli, R.; Powell, A. K. Dysprosium triangles showing single-molecule magnet behavior of thermally excited spin states. *Angew. Chem., Int. Ed.* **2006**, *45* (11), 1729.
(30) (a) Wernsdorfer, W. From micro-to nano-SQUIDs: applications to nanomagnetism. *Supercond. Sci. Technol.* **2009**, *22* (6), No. 064013. (b) Wernsdorfer, W.; Chakov, N.; Christou, G. Determination of the magnetic anisotropy axes of single-molecule magnets. *Phys. Rev. B Condens. Matter* **2004**, *70* (13), No. 132413.
(31) Ling, B.-K.; Zhai, Y.-Q.; Jin, P.-B.; Ding, H.-F.; Zhang, X.-F.; Lv, Y.; Fu, Z.; Deng, J.; Schulze, M.; Wernsdorfer, W.; et al. Suppression of zero-field quantum tunneling of magnetization by a fluorido bridge for a "very hard" 3d-4f single-molecule magnet. *Matter* **2022**, *5* (10), 3485−3498.
(32) Paul, S.; Kotagiri, G.; Ganguly, R.; Subramanian, A.; Courtois, H.; Winkelmann, C. B.; Gupta, A. K. Magnetization reversal across multiple serial barriers in a single Fe 3 O 4 nanoparticle. *Phys. Rev. B* **2022**, *105* (18), No. L180410.

https://doi.org/10.1021/jacs.5c12742
J. Am. Chem. Soc. 2025, 147, 39572−39581